World Academy of Science, Engineering and Technology
International Journal of Chemical and Molecular Engineering
Vol:18, No:9, 2024

Atmospheric Oxidation of Carbonyls: Insight to Mechanism, Kinetic and Thermodynamic Parameters

Olumayede Emmanuel Gbenga, Adeniyi Azeez Adebayo

***Abstract*—**Carbonyls are the first-generation products from tropospheric degradation reactions of volatile organic compounds (VOCs). This computational study examined the mechanism of removal of carbonyls from the atmosphere via hydroxyl radical. The kinetics of the reactions were computed from the activation energy (using enthalpy (ΔH**) and Gibbs free energy (ΔG**). The minimum energy path (MEP) analysis reveals that in all the molecules, the products have more stable energy than the reactants, which implies that the forward reaction is more thermodynamically favorable. The hydrogen abstraction of the aromatic aldehyde, especially without methyl substituents, is more kinetically favorable compared with the other aldehydes in the order of aromatic (without methyl or meta methyl) > alkene (short chain) > diene > long-chain aldehydes. The activation energy is much lower for the forward reaction than the backward, indicating that the forward reactions are more kinetically stable than their backward reaction. In terms of thermodynamic stability, the aromatic compounds are found to be less favorable in comparison to the aliphatic. The study concludes that the chemistry of the carbonyl bond of the aldehyde changed significantly from the reactants to the products.

***Keywords*—**Atmospheric carbonyls, oxidation, mechanism, kinetic, thermodynamic.

I. Introduction

THE reaction of hydroxide radical as an oxidizing agent through the abstraction of a hydrogen atom is an important reaction in atmospheric chemistry for the removal of volatile organic chemicals. Among many other oxidizing species for the removal of anthropogenic pollutants like ozone (O_3), the nitrate radical (NO_3) and halogen, hydroxyl radicals are the most effective oxidizing species [1], [2] because of their high reactivity and their significant and constant tropospheric concentration, i.e., 9.7 x 10^5 radicals cm^{-3} [1]. In aldehydes like formaldehyde and acetaldehyde, the hydrogen abstraction was suggested to possibly take place at the closest H-C to the C=O group while the OH addition channel was found to be unfavorable [3].

In this study, the oxidation reactions of hydroxyl radical for the abstraction of a proton from aldehydes are considered. A schematic representation of the oxidation reaction of the *OH for the abstraction of a hydrogen atom from aldehydes is shown in Fig. 1. The 11 models of aldehyde derivatives that were considered in this study include seven aliphatic (M1 to M7) and four aromatic aldehydes (M8 to M11) are shown in Fig. 2.

Emmanuel Gbenga Olumayede is with the Federal University Oye-Ekiti, Nigeria (e-mail: emmauel.olumayede@fuoye.edu.ng).

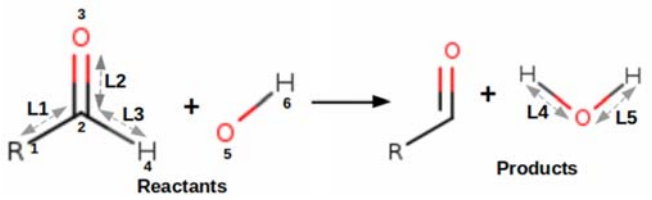

Fig. 1 The schematic representation of the OH abstraction of the aldehyde hydrogen atom showing the selected bond representation and numbering of atoms of interest

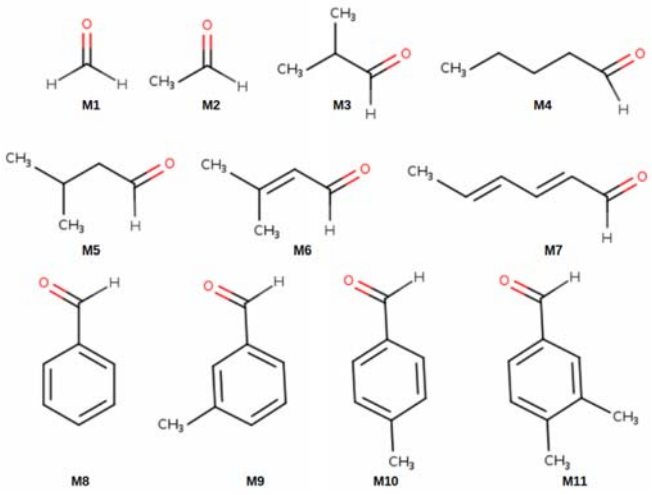

Fig. 2 The schematic representation of the 11 derivatives of the aldehydes that were examined for the hydrogen abstraction reaction. The 11 modeled aldehydes are Formaldehyde (M1), Acetaldehyde (M2), 2-Methylpropionaldehyde (3M), Pentanaldehyde (4M), isoPentanaldehyde (M5), 3-Methyl-2-butenal (M6), 3-Methyl-2-butenal (M7), Benzaldehyde (M8), 3-Methylbenzaldehyde (M9), 4-Methylbenzaldehyde (M10) and 2,4-diMethylbenzaldehyde (M11)

II. Methodology

A. Computational Methodologies

All the geometries of the reactions were optimized using hybrid density functional theory (DFT) B3LYP and the basis set def2-TZVP [4] as implemented in Orca 4.2 package [5], [6]. The reaction paths from reactant to product were followed using Nudged-Elastic-Band (NEB) method [7], [8] to locate the saddle point which was then optimized to transition state. The same hybrid functional method B3LYP and basis set def2-TZVP was used for NEB calculation and atom-pairwise dispersion correction D4 [9] was applied.

The population analysis of the electron and the wavefunction that were used to compute other properties of the molecules in their optimized stationary state of reactant,

transition and product states were computed using the functional method B3LYP and basis set 6-31+G(2df,2p) in the Gaussian 16 package [10].

The interaction energy (ΔE_{int}) of the fragments of reactants, products and their transition state were calculated using natural energy decomposition analysis (NEDA). The NEDA method as described in our previous work [11] was based on five partitions of the SCF interaction defined by Kitaura and Morokuma [12], [13] using functional HF and basis set DEF2SVP.

The obtained wavefunction file was used to compute the molecular electrostatic potential (MESP) values as implemented in Multiwfn program [14]-[16] using the standard equation for molecular electrostatic potential V(r) at a point r:

$$V(r) = \sum_A^N \frac{Z_A}{|r-R_A|} - \frac{\rho(r\prime)d^3r\prime}{|r-r'|}$$

The Z_A, R_A and $\rho(r')$ in the expression stand respectively for the nucleus, position and electron density. The minima (V_{min}) critical points (CP) of MESP corresponds to (3, +3) CP; the maxima (V_{max}) represented by (3, -3); while the saddle points are designated with (3, +1) and (3, -1) designate [17]. The V_{max} is known does not to exist in the three dimensions of the MESP surface as the only possible existence of V_{max} is associated with the nuclei [18]-[21], the reported V_{max} in this work represent only the most positive (highest values) on the MESP surface [22]-[24].

The Arrhenius equation is used to estimate the rate constant (k) from the activation energy ($\Delta E^{\ddagger}$) as:

$$k = Aexp\left(\frac{-\Delta E^{\ddagger}a}{RT}\right)$$

The R is gas constant (0.00831447 $kJK^{-1}mol^{-1}$) and T is the temperature in Kelvin.

III. Results and Discussion

A. Minimum Energy Path

The computed MEP for the abstraction of a proton from all of the 11 derivatives of the aldehydes is shown in Fig. 3. In all of the molecules, the products have more stable energy than the reactants, which implies that the forward reaction will be thermodynamically favorable for the abstraction H atom from aldehyde by OH^- to form water molecule.

The feature of the change in the geometry of the molecules along the MEP is shown in Fig. 4 for derivative M11 with hydroxyl radical. As can be observed, the *OH is approaching the aldehyde, the bond angle that connects the C=O to the rest of the aldehyde (L1-L2 as shown in scheme 1) first experience relaxation of the bond angle L1-L2 (124.99^0 to 126.99^0), thereafter the same bond angle begins to experience compression around the TS structure formation (125.38^0) and then followed by expansion after the abstraction of the proton (130.18^0) to form the product (130.07^0). In summary, the bond angle L1-L2 is higher in the product than the reactant. The C=O bond (L2) experience a little compression from the reactant to products (1.22 to 1.19 Å). Also, the O-H bond (L5) experience a little compression from the reactant to the product (0.99 to 0.96 Å).

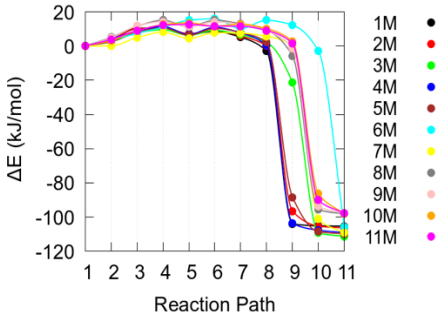

Fig. 3 The reaction path from the reactants to product for the abstraction of a proton from the 11 derivatives of the aldehydes

Also worthy of note in Fig. 4 is that the L3 bond did not shown any significant change from the reactant to transition state but start undergoing elongation from transition state to products while L4 keep undergoing compression from reactant to product to form a water molecule. The two reaction path bonds (L3 and L4) were not changing simultaneously until the transition state geometry was formed.

A. The Kinetics of the Reactions

The changes in activation barrier energies for the forward (E_{TS} - E_{rxt}) and reverse reactions (E_{TS} – E_{pdt}) of the compounds were examined using ΔH^{**} and ΔG^{**} of the reactions as the temperature changes from 268.15 to 318.15 K. Generally, the activation energy is much lower for the forward reaction than backwards using the results from both enthalpy and Gibbs free energy. This is an indication that the forward reactions are more kinetically favorable than their backward reaction. The plot of the reaction rate computed using CVT/SCT are shown in Fig. 5 for the forward reaction and reverse reaction. The H abstraction show overall negative temperature dependence, as the rate of H abstraction was higher at lower temperature than higher temperature. This agree well with many of the previous experimental and computational studies as reported in the literature [3]. In the reverse reaction, the observation is different from forward reaction as it is found to be more temperature dependent (Fig. 4b) (excluding the aromatic M8-M11 that appears to be parabolic) which is also the same pattern in the equilibrium constant.

At lower temperature, significant differences are observed in the reaction rate of the molecules. On top of every other molecules is the aromatic aldehyde M8 that have the highest rate in the order of M8 > M9 > M1 > M10 > M3 > M11 > M2 for the forward reaction while the reverse reaction is in the order of M8 > M1 > M3 > M2 > M7. This implies that the forward reaction favors abstraction of H from aromatic aldehyde with no methyl substituent or with only one methyl substituent especially at meta position (M8 and M9) and also favors short chain alphatic aldehydes like M1, M2 and M3. The longer chain alphatic aldehydes (M4, M5) disfavored the

H abstraction reaction and also the presence of two methyl groups on the aromatic aldehydes (M11). The diene aldehyde (M6 and M7) have poor reaction rate kinetic for the abstraction of H atom.

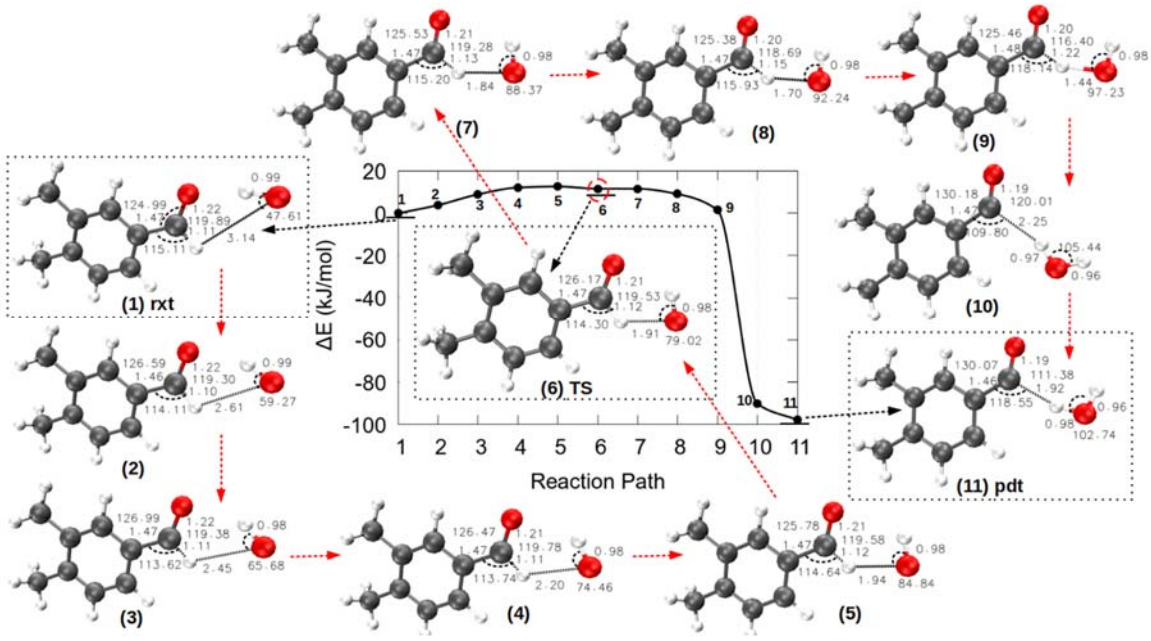

Fig. 4 The change in the geometry along the reaction MEP for the proton abstraction from 2,4-diMethylbenzaldehyde (11M) by hydroxyl radical shown the change in the selected bond distances and angles of interest; the geometry of the reactants, transition state and product are enclosed in a dotted box

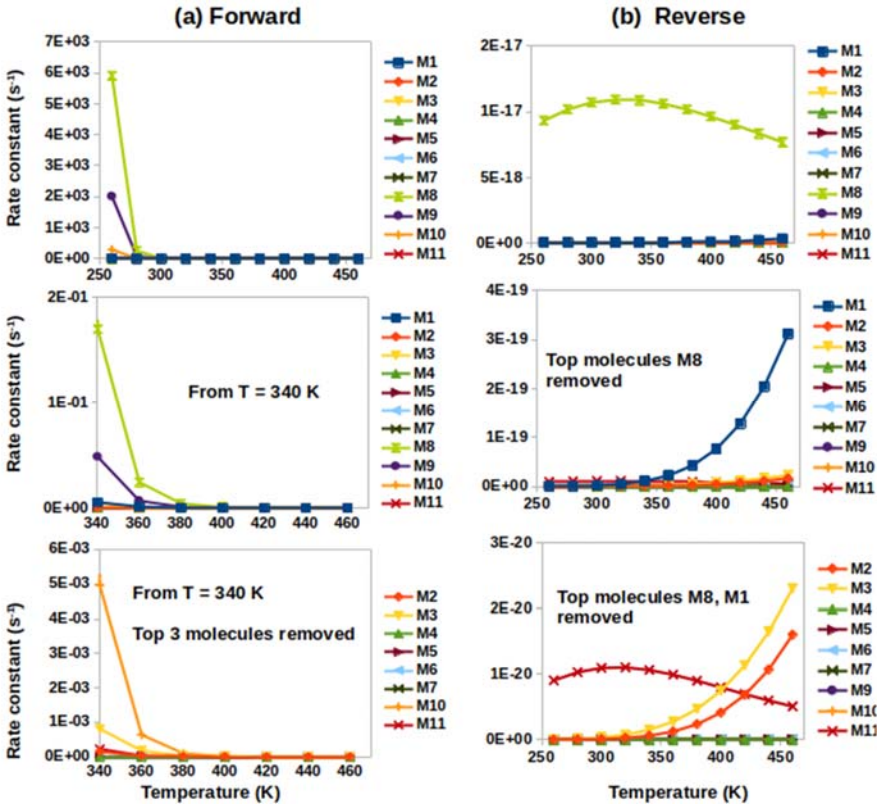

Fig. 5 The plot of the reaction rate using canonical variational transition state theory (CVT) and small-curvature tunneling (SCT) for the (a) forward reaction and (b) reverse reaction

B. The Effects of the Thermodynamic Changes

In terms of thermodynamic stability, the aromatic compounds are found to be less favorable in comparisons to the aliphatic using the results from ΔE, ΔH and ΔG. Entropy favors the thermodynamic stability of the product involving branched alkane (M5) compare to straight-chain alkane (M4). The order of thermodynamically favorability is not the same with how they were kinetically favored as many of the molecules that favor the H abstraction reaction (M1, M2, M3, M8, M9, M11) are not list among the most thermodynamically favorable molecules according to their (M1, M3, M5 and M7).

C. The OH Radical and Aldehyde Interactions

The values of the contribution of polarizability, charge transfer, electrostatic, electricity and core electron to the total interaction energy of the two fragments are shown in Table I. The interaction of the two fragments in the reactants is characterized by lower energy of interactions (ΔE_{int}) compare to the transition state and the product (Fig. 6 (a)). The lower energy of interaction of the reactants is an indication that the reaction will proceed forward more favorably which is also supported with lower kinetics of the forward reaction. Among all the molecules, the compound M3, M5 and M6 have the lowest energy of interaction compare to the rest of the molecules and were also among those listed to be thermodynamically favored. Those with the lowest ΔE_{int} are also characterized with the lowest charge transfer (Fig. 6 (b)), electrical and electrostatic (Table I).

TABLE I
THE ELECTROSTATIC (ES), ELECTRICAL (EL), POLARIZABILITY (POL), CHARGE TRANSFER (CT), CORE ELECTRON AND TOTAL INTERACTION (ΔE_{INT}) ENERGIES (IN KCAL/MOL) FOR THE INTERACTIONS OF THE TWO FRAGMENTS IN THE REACTANT, TRANSITION STATE AND PRODUCTS OBTAINED USING NEDA ANALYSIS

Mol	ES	POL	EL	CT	Ex	Core	ΔE_{int}
Reactants							
M1	-9.150	-2.931	-10.623	-11.044	-1.523	17.119	-4.548
M2	-10.773	-3.419	-12.493	-13.227	-1.719	20.211	-5.509
M3	-87.071	-6.851	-90.678	-34.627	-2.045	32.677	-92.628
M4	-11.049	-3.499	-12.807	-13.694	-1.751	20.845	-5.656
M5	-86.791	-6.935	-90.552	-45.680	-1.983	38.375	-97.857
M6	-81.692	-6.982	-85.423	-22.763	-2.234	32.266	-75.920
M7	-11.415	-4.747	-13.703	-15.549	-1.735	26.565	-2.687
M8	-11.697	-3.790	-13.587	-14.691	-1.852	22.167	-6.112
M9	-11.919	-3.832	-13.831	-15.056	-1.871	22.755	-6.132
M10	-12.042	-3.955	-14.009	-15.275	-1.906	23.050	-6.234
M11	-12.267	-3.914	-14.219	-15.544	-1.914	23.347	-6.417
Transition state							
M1	-5.860	-5.404	-8.551	-11.189	-3.031	20.562	0.822
M2	-7.337	-6.663	-10.649	-13.771	-3.819	25.243	0.823
M3	-7.402	-6.507	-10.635	-13.174	-3.744	23.843	0.034
M4	-7.281	-6.456	-10.488	-13.121	-3.694	23.840	0.232
M5	-7.462	-6.896	-10.913	-9.913	-3.845	27.323	6.496
M6	-8.431	-7.101	-11.947	-14.911	-4.075	26.864	0.006
M7	-7.492	-7.557	-11.214	-14.951	-4.103	29.864	3.699
M8	-11.331	-6.015	-14.364	-15.535	-4.776	33.594	3.695
M9	-11.564	-6.164	-14.667	-16.034	-4.882	33.522	2.821
M10	-11.912	-5.918	-14.916	-16.226	-4.946	35.592	4.450
M11	-11.715	-6.240	-14.856	-16.145	-4.916	33.801	2.801
Products							
M1	-3.244	-2.830	-4.661	-3.673	-1.159	7.315	-1.019
M2	-4.073	-2.630	-5.401	-8.665	-1.336	13.633	-0.433
M3	-4.889	-3.028	-6.417	-11.081	-1.571	16.979	-0.519
M4	-4.637	-2.780	-6.043	-10.759	-1.467	16.392	-0.410
M5	-4.330	-2.794	-5.738	-10.705	-1.398	16.235	-0.208
M6	-4.911	-3.209	-6.517	-9.854	-1.364	15.010	-1.361
M7	-5.659	-3.250	-7.294	-11.914	-1.803	18.438	-0.770
M8	-5.049	-3.342	-6.729	-11.387	-1.777	17.580	-0.536
M9	-4.973	-3.189	-6.581	-11.411	-1.737	17.904	-0.088
M10	-5.084	-3.206	-6.697	-11.271	-1.739	17.421	-0.547
M11	-4.995	-3.152	-6.582	-11.578	-1.694	17.696	-0.464

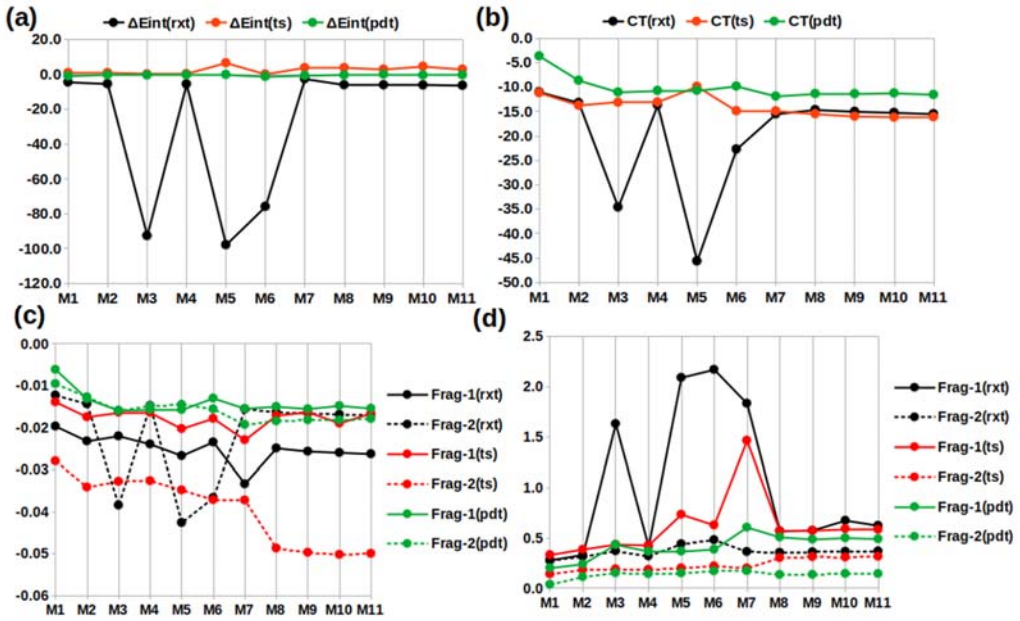

Fig. 6 (a) Fragment interaction energy (ΔE_{int}) (kcal/mol), (b) Charge transfer, (c) the induce energy of the fragments (au) (d) induce dipole of the two fragments

The induced energy of fragment 1 is lower than those of fragment 2 (*OH) in the reactants except for those of M3, M5 and M6 (Fig. 6 (c)) which were also characterized with the lowest values of CT, EL, ES and ΔE_{int} energies as previously discussed. The induced energy of fragment 2 of the transition state is the lowest especially those of the aromatic models compare to other induced energy of the fragments in reactants (except for fragment 2 of M3, M5 and M6) and products. The fragments of the product have relatively small induced energy compare to reactants and transition state. The induced dipole of the fragments is higher in M3, M5, M6 and M7 for fragment 1 of the reactant and also for that of the transition state (excluding M3) (Fig. 6 (d)).

The branched alkane (M5) has better interaction compare to straight-chain alkane (M4) and the branched is also accompanied with better CT, EL, POL, ES (Table I), induce energy and higher induced dipole of aldehyde fragment (fragment 1, Figs. 6 (c) and (d)).

D. Change in the Molecular Orbital

The typical example of the location of the HOMO and LUMO for the molecule M1 and M11 are shown in Fig. 7. In the reactant, the LUMO is located on the OH while the HOMO is on the aldehyde which is well separated from each other especially in molecule M11 which is the reason for the observed higher distance of the centroid in the reactant and hence lower overlap of the orbital and lower bandgap of the reactants. A well-separated HOMO and LUMO will results in a lower repulsion of the electrons and consequently lead to a lower bandgap. In the products, the bandgap is higher due to a higher overlap of the HOMO and LUMO orbitals (Fig. 7) because of poor separation between them as they are both found predominantly on the aldehyde unit (Fig. 7). There is no significant difference between the straight-chain aliphatic molecule (M4) and the branched (M5) in terms of the BG but the difference becomes significant in the presence of double bond (M6 and M7). In the presence of two double bonds, a lower BG that is accompanied by relatively lower overlap orbital, higher orbital separation distance, higher HOMO and LUMO energy is observed compared to other molecules of the same number of carbon (M4, M5 and M6).

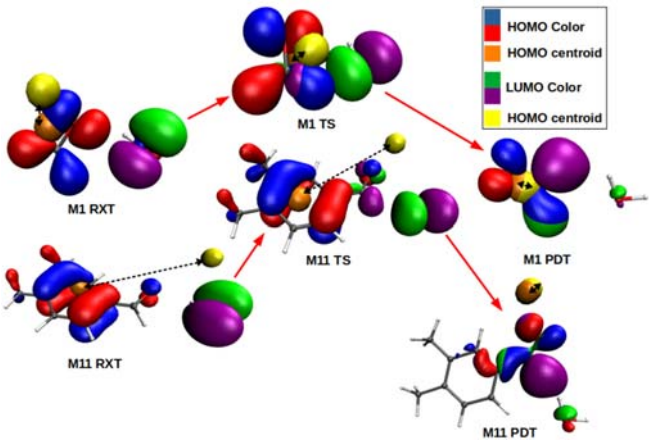

Fig. 7 The HOMO (red and blue) and LUMO (purple and green) orbital so f molecule M1 and M11 showing the calculated distance between the centroid of HOMO (pink) and the centroid of LUMO (yellow). The black arrow shows the calculated distance between the centroids

E. The MESP Properties

Comparing the reactant to product and transition state, the V_{min} is lowest in the reactant than the two other states indicating that the site of V_{min} in the reactant is more available for reaction than those of the transition state and product. The $V_{(C)}$ for the carbon atom of the carbonyl group is also lower in

the reactant than the transition and product state except for molecule M1. There is no direct correlation between the $V_{(C)}$ and its $Q_{(C)}$ but the molecules M6 and M7 that have the lowest $V_{(C)}$ were also characterised with the lowest $Q_{(C)}$ in the reactant, transition and product states of the molecules.

The change in the V_{min} and $V_{(C)}$ across the 11 molecules shows the effect of aldehyde type on the availability of the reaction site especially V_{min} for the reaction. Among all the molecules, M7 has the lowest value of V_{min} of the reactants indicating the effect of the conjugated double bonds on the reaction of the aliphatic aldehyde. Increasing the carbon chain length also lower the V_{min} when considering M1 to M4 while branching increase the V_{min} as seen in M5 but the presence of double bond lowers it as seen in M6. The presence of the para-substituted methyl group helps in lowering the V_{min} of the aromatic aldehyde as seen in M10 compares to metal substitution (M9 and M11).

In the reactant and transition state, the V_{min} is located on the oxygen atom of the hydroxyl radical while the V_{max} is located on the aldehyde hydrogen atoms as shown in Fig. 8. This is an indication that the OH radical drives the reaction as it is the most reactive site of the reactants. In the product, the position of the V_{min} and V_{max} are located on the water molecule while the product of the de-protonated aldehyde has neither.

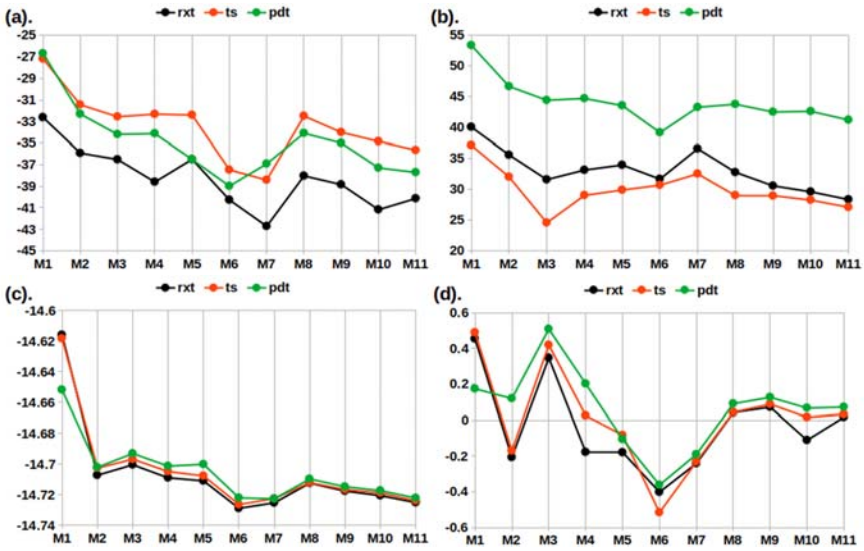

Fig. 8 The MESP (a) V_{min} (b) V_{max} (c) $V_{(C)}$ and (d) atomic charge of the carbon atom ($Q_{(C)}$) of C=O group across the eleven molecules in their reactant, transition and product states

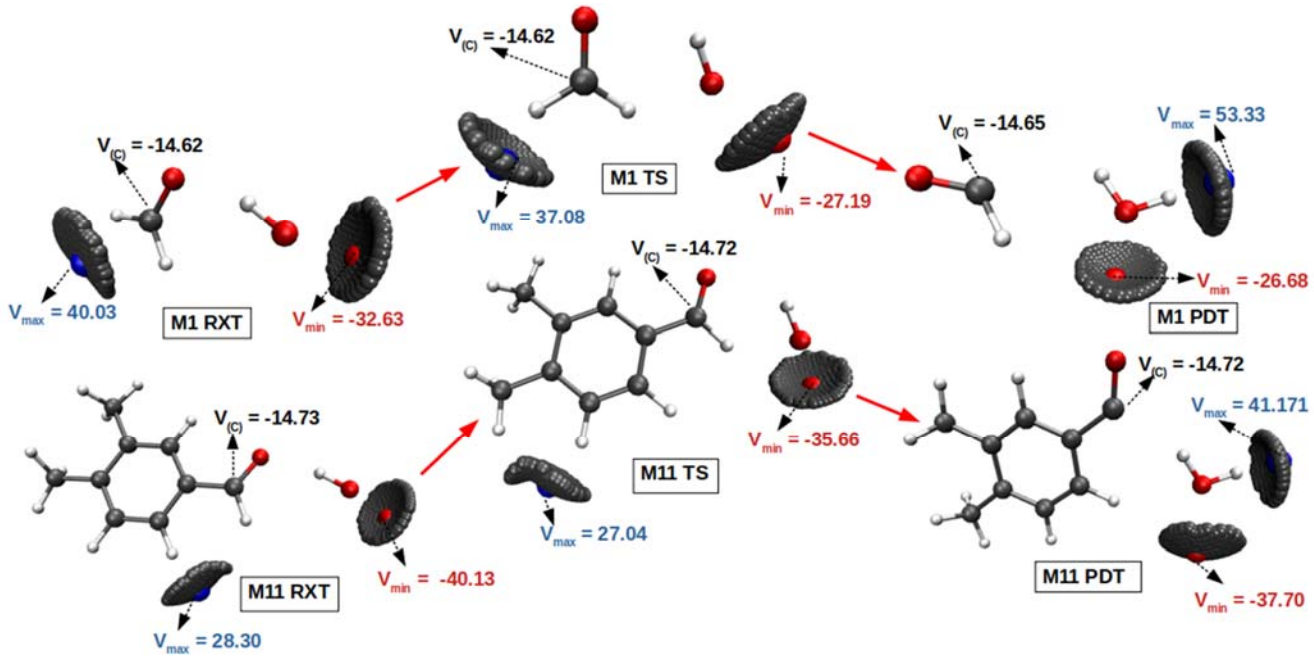

Fig. 9 The MESP analysis of molecule M1 and M11 in their reactant (RXT), transition (TS) and product (PDT) states showing the position of the MESP minimum (V_{min} in kcal/mol), maximum (V_{max} in kcal/mol) and the carbon atom of the carbonyl unit ($V_{(C)}$ in au)

IV. Conclusion

This computational study examined the mechanism and the condition that will favor the removal of the volatile organic chemicals from the atmosphere through their reaction with hydroxide radical as an oxidizing agent. The results can be summarized as follows:

- The MEP analysis shows that the products of the reaction are thermodynamically more stable than the reactant and all the aliphatic aldehyde derivatives gave a relatively more thermodynamically stable product compare to aromatic derivatives as evident from the lower energy of the products of aliphatic compare to those of aromatic.
- The hydrogen abstraction of the aliphatic aldehydes especially the short chain aliphatic aldehyde molecule is more kinetically favorable compare to the longer chain alphatic aldehyde and diene aldehydes.
- The aromatic aldehyde compounds without methyl substituent is ranked the most kinetically favored molecules for H abstraction and the presence of methyl group tends to decrease the kinetic significantly.
- Entropy favors the thermodynamic stability of the product involving branched alkane (M5) compare to straight-chain alkane (M4) and the aromatic compounds are found to be less favorable comparisons to the aliphatic.
- The NEDA analysis of the interaction energy of the aldehyde and hydroxide radical also shows that a more favorable interaction of the reaction species is obtained for those that are thermodynamically favorable and better interaction energy is obtained between the components of reactants than those of the products.
- The HOMO of the reactant is predominantly located on the aldehyde fragment while the LUMO resides on the hydroxyl radical but in the products, they are both predominantly located on the abstracted aldehyde fragment leading to increasing overlap and higher bandgap compare to the reactant.
- The MESP analysis further shows that the reaction site in the reactant is more readily available for reaction than those of the transition state and product because of lower V_{min} found in the reactant compare to the products and transition state.

References

[1] Kovacevic G., Sabljic A. (2017). Environ Sci Process Impacts 19:357–369. doi: 10.1039/c6em00577b
[2] Vereecken L., Glowacki D. R., Pilling M. J. (2015). Chem Rev 115:4063–4114. doi: 10.1021/cr500488p
[3] Alvarez-Idaboy J. R., Mora-Diez N., Boyd R. J., Vivier-Bunge A. (2001). J Am Chem Soc 123:2018–2024. doi: 10.1021/ja003372g
[4] Weigend F., Ahlrichs R. (2005). Phys Chem Chem Phys 7:3297. doi: 10.1039/b508541a
[5] Neese F. (2018) Software update: the ORCA program system, version 4.0. Wiley Interdiscip Rev Comput Mol Sci 8: doi: 10.1002/wcms.1327
[6] Neese F. (2012) The ORCA program system. Wiley Interdiscip Rev Comput Mol Sci 2:73–78. doi: 10.1002/wcms.81.
[7] Henkelman G., Uberuaga B. P., Jónsson H. (2000). J Chem Phys 113:9901–9904. doi: 10.1063/1.1329672
[8] Henkelman G., Jónsson H. (2000). J Chem Phys 113:9978–9985. doi: 10.1063/1.1323224
[9] Caldeweyher E., Bannwarth C., Grimme S. (2017). J Chem Phys 147: doi: 10.1063/1.4993215
[10] Frisch M. J., Trucks G. W., Schlegel H. B., et al (2016) Gaussian 16, Revision B.01,
[11] Adeniyi A. A., Akintayo C. O., Akintayo E. T., Conradie J. (2020). Struct Chem 31:861–875. doi: 10.1007/s11224-019-01470-2
[12] Kazuo K., Keiji M. (2004). Int J Quantum Chem 10:325–340. doi: 10.1002/qua.560100211
[13] Glendening E. D., Streitwieser A. (1994). J Chem Phys 100:2900–2909. doi: 10.1063/1.466432
[14] Lu T., Chen F. (2012). J Comput Chem 33:580–592. doi: 10.1002/jcc.22885
[15] Lu T., Chen F. (2012). J Mol Graph Model 38:314–323. doi: https://doi.org/10.1016/j.jmgm.2012.07.004
[16] Gadre S. R., Shirsat R. N. (200AD) Electrostatics of Atoms and Molecules. Universities Press, India
[17] Gadre S. R., Pathak R. K. (1990). Proc Indian Acad Sci - Chem Sci 102:189–192. doi: 10.1007/BF02860157
[18] Gadre S. R., Kulkarni S. A., Pathak R. K. (1991). J Chem Phys 94:8639. doi: 10.1063/1.460055
[19] Gadre S. R., Kulkarni S. A., Shrivastava I. H. (1992). J Chem Phys 96:5253–5260. doi: 10.1063/1.462710
[20] Politzer P., Murray J. S. (2002). Theor Chem Acc 108:134–142. doi: 10.1007/s00214-002-0363-9
[21] Politzer P., Murray J. S., Peralta-Inga Z. (2001) Int J Quantum Chem 85:676–684. doi: 10.1002/qua.1706
[22] Li W., Yang N., Lyu Y. (2016) Org Chem Front 3:823–835. doi: 10.1039/c6qo00085a
[23] Kaul D., Kaur R. (2015). J Chem Sci 127:1299–1313. doi: 10.1007/s12039-015-0885-z
[24] Zhao Y., Truhlar D. G. (2008). Theor Chem Acc 120:215–241. doi: 10.1007/s00214-007-0310-x